γ-ray spectra from positron annihilation on atoms and molecules

Koji Iwata, R. G. Greaves, and C. M. Surko
Physics Department, University of California, San Diego, La Jolla, California 92093-0319
(Received 23 October 1996)

Positron annihilation on a wide variety of atoms and molecules is studied. Room-temperature positrons confined in a Penning trap are allowed to interact with molecules in the form of low-pressure gases so that the interaction is restricted to binary encounters between a positron and a molecule. Data are presented for the γ-ray spectra resulting from positrons annihilating in such interactions. The Doppler broadening of these spectra is a measure of the momentum distribution of the annihilating electron-positron pairs. Consequently, these spectra provide information about the electron and positron wave functions. Systematic studies of annihilation line shapes are discussed for noble gases, a variety of inorganic molecules, alkanes, alkenes, aromatics, and perfluorinated and partially fluorinated hydrocarbons. In the case of molecules, the measurements are used to determine the probability of positrons annihilating at specific locations in the molecule. For example, in the case of partially fluorinated hydrocarbons, we have been able to determine the relative probability of annihilation on the fluorine atoms and on the C-H bonds. Insights that these studies provide in understanding the interaction of low-energy positrons with atoms and molecules are discussed. [S1050-2947(97)05405-X]

PACS number(s): 34.50.−s, 78.70.Bj, 71.60.+z, 36.10.−k

I. INTRODUCTION

The interactions of low-energy positrons with matter have been studied extensively [1,2]. In some respects, positrons interact with matter in ways that are similar to those of electrons because of the identical masses of an electron and a positron. However, in other respects they behave very differently because the electron and positron have opposite signs of electric charge and are distinguishable particles. This is generally most noticeable for low-energy interactions since it is in this regime that differences related to the Coulomb interaction and the Pauli exclusion principle play larger roles. In addition, positrons can also exhibit unique processes, namely, positronium atom formation [3] and annihilation with an electron. Central to the work discussed here, positron annihilation can provide information not available from electron-matter interactions. For example, much information about defects near the surfaces of solids can be obtained by studying positron annihilation [4].

The interaction of low-energy positrons with atoms and molecules has been the subject of numerous studies and is currently a field of active research [5–9]. Studies of this kind have many potential applications, for example, in mass spectrometry, where positron annihilation is a qualitatively different way of ionizing molecules [10–12]. Positrons also provide stringent tests of scattering theories. In recent work, three types of positron-molecule measurements have been performed using positrons stored in Penning traps. One type of experiment is measurement of the lifetime of positrons annihilating in a sample gas [7]. Such measurements provide information about annihilation cross sections. Another type of experiment involves measurement of the spectra of positive ions produced as a result of positron annihilation [10,12–14]. In the experiments discussed in this paper, we study the momentum distribution of the annihilating electron-positron pairs by measuring the Doppler broadening of the γ-ray annihilation spectrum [15,16].

Extensive measurements of momentum distributions of annihilating electron-positron pairs have been performed in solid and liquid targets [4], and they provide information about the annihilation processes and other properties of materials. In this paper, this technique is applied to make systematic measurements in gaseous media, which are sufficiently tenuous so that the interaction of positrons with an individual atom or molecule can be isolated and studied.

Earlier measurements of this type were mainly performed in dense or high pressure gases using a different technique from the one described here. In those experiments a positron source (usually a radioactive isotope such as ^{22}Na or ^{66}Co) is placed in a gas cell so that high-energy ($\sim$10–500 keV) positrons are emitted directly into the annihilation medium. The positrons experience energy loss through collisions with the atoms or molecules, eventually reaching thermal equilibrium with the medium. The annihilation γ rays are measured using either high-resolution Ge detectors or the angular correlation technique, described in Sec. II. In general, the thermalization time is shorter than the annihilation time scale so that studies of free positron annihilation on molecules at the temperature of the medium are possible. One disadvantage of this method is that positronium atom formation can take place during the slowing down of the positrons, and subsequent annihilation of the thermalized positronium atoms can obscure the free positron annihilation signal. Another potential complication is that, in condensed gases or high pressure gases, it is difficult to isolate and study the interaction of a positron with a single atom or molecule. For studies of substances in the gas phase, compounds are limited to those that exist in gaseous form at the operating temperature and pressure. In practice, the operating pressure must be suitably high so that the positrons stop in the test media. For those experiments, the sample temperatures are typically room temperature or lower, while the pressure is typically atmospheric pressure or larger.

We have been able to avoid these shortcomings by the use of positrons accumulated and cooled in a Penning trap [17], where they are confined by a combination of magnetic and

 © 1997 The American Physical Society

electrostatic fields. Positronium atom formation is avoided since the positrons can be cooled below the formation threshold before the sample gas is introduced. This technique can be used at low sample gas pressure ($<10^{-6}$ torr) so that substances that exist as liquids or solids at room temperature can be introduced into the trap as low-pressure vapors.

In addition to their application for studies of positron-molecule interactions, stored positrons have also been used for a variety of other experiments, including studies of electron-positron plasmas [18]. They also have the potential for supplying positrons for antihydrogen formation [19–21].

Previous experiments of Doppler-broadened γ-ray spectra in Penning traps [15,16] demonstrated the feasibility of the use of stored positrons for spectral measurements. Subsequent improvements in positron moderation [22,23] and trapping efficiency as well as in the gas handling system have now enhanced the signal-to-noise ratio by 2 orders of magnitude. This has permitted a range of new experiments, including detailed comparison of the annihilation line shape with theoretical calculations [24], the simulation of astrophysical positron annihilation [25], and the localization of the sites of positron annihilation in complex molecules.

In this paper, we describe a systematic study of positrons interacting with a wide variety of atoms and molecules. Data are presented for noble gases, inorganic molecules, alkanes, alkenes, aromatics, substituted hydrocarbons, as well as fully and partially fluorinated hydrocarbons. Important results include demonstration of the ability to resolve, for the first time in gaseous media, non-Gaussian features in the line shapes and detection of more than one annihilation site in molecules, including distinguishing annihilation on the C-H bond from that on the fluorine atom in partially fluorinated hydrocarbons. We also present data indicating that, in hydrocarbons, we can distinguish annihilation on the C-H bond from that on the C-C bond. In all molecules studied, the data are consistent with the positrons annihilating predominantly with valence electrons. A study of halogenated hydrocarbons is also presented. It shows that the positrons annihilate on the halogen atoms with a linewidth very similar to that of the related noble gas atom, particularly in the case of the larger halogens. We expect that the systematic studies presented in this paper will provide useful constraints on theories of low-energy positron-atom and positron-molecule interactions.

This paper is organized in the following manner. In Sec. II, we review previous experiments to measure the momentum distributions of annihilating electron-positron pairs. The experimental setup is described in Sec. III. The results of the experiments are described in Sec. IV, including the results of an extensive study of partially fluorinated hydrocarbons and a simulation of astrophysical positron annihilation. Detailed analyses of spectral line shapes are then presented in Sec. V. In Sec. VI, we discuss the implications of the results presented in this paper for current theoretical work and for progress in other areas of positron-molecule interactions. A brief set of concluding remarks is presented in Sec. VII.

II. MOMENTUM DISTRIBUTION MEASUREMENTS

An electron-positron pair annihilates by emitting two quanta of 511-keV γ rays at an angle of 180° in the center-of-mass frame of the two particles. However, in the laboratory frame, the γ rays carry away the initial momentum of the center of mass of the pair. Thus, as illustrated in Fig. 1, the angle of emission of the two photons relative to one another deviates slightly from 180° due to the perpendicular components of the momentum of the electron-positron pair, p_x and p_y. The γ rays are Doppler shifted in energy due to the longitudinal momentum component of the pair, p_z. When $p_x, p_y \ll m_0 c$, the angle of deviation θ can be expressed as

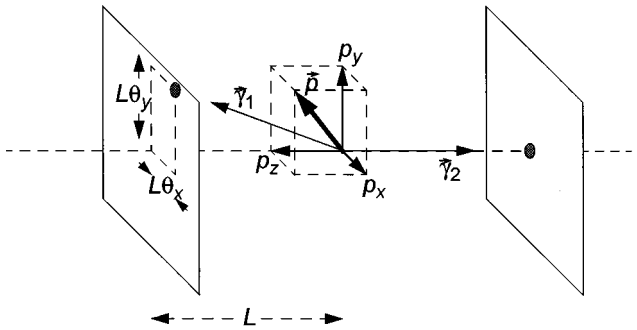

FIG. 1. Illustration of the momentum of an annihilating electron-positron pair $\vec{p}$ and the resulting γ-ray momenta, $\vec{\gamma}_1$ and $\vec{\gamma}_2$. An annihilation event is observed with two detectors placed 180° with respect to the annihilation site at distance L. The longitudinal component of $\vec{p}$, p_z, shifts the energies of γ rays, and the tangential components, p_x and p_y, deflect the γ rays by an angle $\theta=(\theta_x^2+\theta_y^2)^{1/2}$. (The angle of deflection is exaggerated in this figure.)

$$\theta_j \simeq \frac{p_j}{m_0 c}, \tag{1}$$

where $j=x$ or y, m_0 is the rest mass of the electron, and c is the speed of light. The Doppler shift in the energy, ΔE, is given by

$$\Delta E = \frac{p_z}{2 m_0 c} E_0 = \frac{c p_z}{2}, \tag{2}$$

where $E_0 = m_0 c^2$ is the rest mass energy of the electron. The perpendicular components of the momentum of the annihilating pair can be studied by measuring the angular correlation of two γ rays. The longitudinal component can be measured by observing the Doppler broadening of the γ-ray spectrum using high-resolution solid-state detectors such as lithium-drifted or intrinsic germanium detectors.

When annihilation follows thermalization of the positrons in the medium, e.g., with the characteristic energy of $(3/2)kT = 0.04$ eV (corresponding to room temperature), the momentum of the annihilating pairs is typically dominated by the momenta of the electrons. Techniques for measuring these momentum distributions were developed initially for the studies of positron annihilation in condensed media [4]. They have been applied to studies of positron-gas interactions as well [9]. When the medium is a crystalline solid, p_x and p_y can be distinct. For example, the anisotropy in two dimensions has been observed and studied in some materials [26]. When the medium under investigation is a liquid or gas, the momentum distribution is rotationally averaged, and

the three momentum components are equivalent. In this case, the angular deviation θ and the energy spread ΔE are related by

$$\Delta E = m_0 c^2 \frac{\theta}{2}, \tag{3}$$

and angular correlation and Doppler-broadening measurements can be compared.

A. Annihilation γ-ray angular correlation measurements

The technique of angular correlation of annihilation radiation (ACAR) was developed to determine the perpendicular components of the momenta of annihilating electron-positron pairs in solids, liquids, and dense gases [4]. Initially, the measurements were performed in a one-dimensional geometry [27] in which two γ-ray detectors are located behind slit collimators on opposite sides of the annihilation region. One of the detectors is scanned as a function of the angle between the two detectors, and coincident events are recorded. One advantage of the ACAR method is its high resolution. Typical angular resolutions achievable are about 0.65 mrad [28], which is equivalent to the γ-ray energy resolution of 0.2 keV using Eq. (3).

In order to obtain high resolution, the slits must be placed as far from the annihilation cell as possible, typically tens of meters. This results in reduced count rates due to the small solid angle subtended by the detector at the sample. In order to obtain both a large number of counts and high resolution in a reasonable amount of time, one would like to have as many positrons as possible annihilating in a small volume. This condition can be satisfied in solid and liquid targets [29,30], but in this case, annihilation may involve the interaction of a positron with multiple atoms or molecules. In contrast, in gaseous media the two-body assumption is more likely to be met, but ACAR measurements are more difficult because the mean free path of positrons in gases is relatively large and results in a large annihilation region and low count rates. The first ACAR measurements in gaseous media were reported by Heinberg and Page in 1957 [31]. However, their study was focused on positronium atoms in which the information content of the signal is less sensitive to the details of the spectra. The introduction of the two-dimensional (2D) ACAR detector [28] has enabled measurements in the gas phase with significantly increased count rates. For 2D ACAR, two relatively large NaI crystals with position-sensitive detectors attached replace the detector-slit combinations. The position-sensitive detectors can accurately identify the location of scintillations produced by γ rays without much loss of count rate. The measurements in gaseous media using a 2D ACAR detector were reported by Coleman *et al.* [9], and their study showed the first quantitative ACAR results of free positrons annihilating on atoms.

B. Doppler-broadened γ-ray spectral measurements

For the experiments described in this paper, an alternative method of obtaining the momenta of the annihilating electron-positron pairs was used. We measure directly the Doppler broadening of the annihilation line using a high-energy resolution solid-state γ-ray detector (an intrinsic germanium detector) in conjunction with a multichannel analyzer (MCA). This yields the longitudinal component, p_z, of the annihilating pair's momentum, which is equivalent to either of the other two components in an isotropic medium such as a gaseous target. An advantage of the Doppler-broadening technique is that a high count rate can be obtained since the detector can be placed close to the annihilation region, and this results in a large collection solid angle. This permits measurements in diffuse media, such as low-pressure gases [15,16,32]. Another advantage of this technique is the compactness of the equipment and the ease of installation. As described in Sec. IV J, this technique can also be applied to studies of positron annihilation in the interstellar medium, where ACAR techniques are inapplicable. However, a disadvantage of the Doppler-broadening measurements is their relatively poor resolution. For example, an intrinsic Ge detector typically has the energy resolution of $\sim$1 keV at 511 keV as compared with the equivalent ACAR resolution of 0.2 keV discussed above. In the experiments described here, an intrinsic Ge detector is used to take advantage of the high count rate in diffuse media where positrons are interacting with low-pressure gas atoms or molecules.

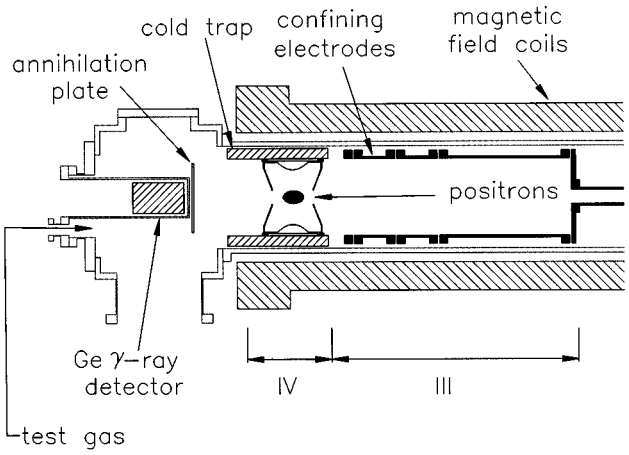

FIG. 2. Schematic diagram of the last two stages of the positron trap and the detector.

Lynn *et al.* employed an improved implementation of the Doppler-broadening approach, which utilizes two high-resolution Ge detectors placed 180° with respect to the annihilation region [33]. This technique can dramatically increase the signal-to-noise ratio of the data. Use of this technique allowed them to detect positron annihilation on inner-shell electrons in condensed media. This method can, in principle, be used for studies of positron annihilation in gaseous media, which is discussed in Sec. VI.

III. DESCRIPTION OF THE EXPERIMENT

A. The positron trap and gas handling procedures

The experiments were performed using a technique similar to that discussed previously [16]. The schematic layout of the experiment is shown in Fig. 2. Positrons emitted from a 60-mCi ^{22}Na radioactive source at a spectrum of energies up to 540 keV are moderated to a few electron volts by a solid neon moderator [22,23]. They are then accelerated to about

30 eV and guided by a magnetic field into the four-stage Penning trap. The trap consists of a vacuum chamber surrounded by a solenoid that provides positron confinement in the radial direction and an electrode structure that provides electrostatic confinement in the axial direction. The positrons experience inelastic collisions with nitrogen buffer gas molecules introduced into the first stage of the trap. These collisions result in the positrons being trapped in the potential well created by the electrodes. More detailed descriptions of the operation of the positron trap are presented elsewhere [34,35].

Positrons accumulated in the third stage of the trap cool to room temperature in approximately 1 s by electronic, vibrational, and rotational excitation of nitrogen molecules. The positrons are then shuttled to the fourth stage, where the N_2 pressure is the lowest and where the positrons are closer to the γ-ray detector. The trap protocol is designed to accumulate an optimal number of positrons with minimal losses from annihilation on buffer gas molecules. A cold trap, shown in Fig. 2, is filled either with liquid nitrogen or with a water-ethanol mixture chilled to $-7\,^{\circ}$C in order to reduce impurities in the vacuum system. The base pressure of our system is typically 5×10^{-10} torr, and the positron lifetime with the buffer gas turned off is typically 1 h with liquid nitrogen in the cold trap and a few minutes with the chilled water-ethanol mixture. Liquid nitrogen in the cold trap can be used only for gases that do not condense at 77 K. Measurements of some of the substances, obtained with liquid nitrogen in the cold trap, were repeated with the chilled water-ethanol mixture. No difference in the spectra was detected except that higher count rates were observed when liquid nitrogen was used.

The experiment is operated in a series of repeated cycles of positron filling and annihilation. In each cycle positrons are accumulated for a fixed period of time (typically 5 s) in the presence of the N_2 buffer gas. The buffer gas is then shut off, following a positron cooling time of 1 s. The buffer gas pressure is then allowed to drop for another 8 s. The intrinsic Ge detector is gated on, and the test gas is introduced. Typically, the spectrum is accumulated on the MCA for 5 s in the presence of the test gas, and then the test gas is turned off. This cycle is continued for about 12 h to accumulate a large number of counts, with the total counts in the peak typically $\sim10^6$. The number of positrons in the trap and the pressures of the test gases are carefully adjusted to obtain the highest count rates consistent with avoiding γ-ray pileup, which can distort the shape of the spectrum.

The positron temperature is measured separately. The depth of the confining potential well is lowered slowly, and the number of positrons escaping from the trap is analyzed to measure the positron temperature. This technique is described in detail elsewhere [36]. We find that the positrons are at room temperature (i.e., ~300 K).

Small amounts of impurities with high annihilation rates in test substances can greatly affect the experimental results [7]. We have used substances with highest purity commercially available (generally $>99.9\%$), and the annihilation contribution from impurities is less than 1%. Some of the substances have additives for various reasons, and appropriate treatments were used to remove them. For example, commercially available acethylene contains acetone. We placed a cold trap in the gas line to remove this impurity.

B. Spectral analysis

We have found a Gaussian line shape to be a useful fitting function for both the detector calibration lines and the annihilation spectra observed from atoms and molecules. In practice, the fitting function also contains a complementary error function component, which models Compton scattering in the detector crystal [37], and a constant background. This fitting function has the form

$$f(E)=A_1\exp\left[-\left(\frac{E-E_0}{a\Delta E_{\rm fit}}\right)^2\right]+A_2\,\mathrm{erfc}\left(\frac{E-E_0}{a\Delta E_{\rm fit}}\right)+A_3, \quad (4)$$

where E is the γ-ray energy, $\Delta E_{\rm fit}$ is the full width at half maximum (FWHM) of the line, $a=1/(4\ \ln 2)^{1/2}$, A_1 and A_2 are amplitudes, A_3 is the background, and $\mathrm{erfc}(x)$ is the complementary error function. The fit parameters are A_1, A_2, A_3, E_0, and $\Delta E_{\rm fit}$. Representing the counts in each energy bin E_j by y_j, the quantity minimized is

$$\chi_r^2=\frac{1}{N-k}\sum_{j=1}^{N}\left[\frac{y_j-f(E_j)}{\sigma_j}\right]^2, \quad (5)$$

where $\sigma_j=y_j^{1/2}$, N is the number of bins used in the fit, and k is the number of fitting parameters. The value of χ_r^2 is used as a measure of goodness of the fit and is expected to be of order unity for a fit with a good model. The fitting function given by Eq. (4) is a good approximation for the calibration γ-ray lines because the number of free electron-hole pairs produced by a monoenergetic γ ray in a germanium crystal has a Gaussian distribution. For calibration we used essentially monoenergetic γ rays emitted from test sources.

To first order, we have found that the annihilation lines can also be analyzed by fitting Eq. (4). While this is a convenient way of characterizing and comparing data, there is no *a priori* reason that the annihilation lines should have Gaussian line shapes. As discussed in Sec. IV, our data are now of sufficiently high quality to be able to resolve departures from Gaussian line shapes. The measured annihilation line is the convolution of the intrinsic annihilation line shape and the detector response. Under the assumption of Gaussian line shapes, the intrinsic FWHM, ΔE, is given by

$$\Delta E=(\Delta E_{\rm fit}^2-\Delta E_{\rm det}^2)^{1/2}, \quad (6)$$

where $\Delta E_{\rm det}$ is the detector linewidth and $\Delta E_{\rm fit}$ is the fitted linewidth from Eq. (4). The linewidths quoted in this paper are the values of ΔE obtained in this way. In Sec. V, we discuss other attempts (i.e., beyond the one-Gaussian approximation) to fit the measured spectra.

C. Calibration and detector response

The energy scale of the detector response was calibrated using 344.3- and 661.6-keV γ-ray lines from ^{152}Eu and ^{137}Cs test sources, respectively. The lines are fit with Eq. (4) to obtain the centroids and linewidths of the two peaks. The centroids are used to calibrate the energy scale of the spectra,

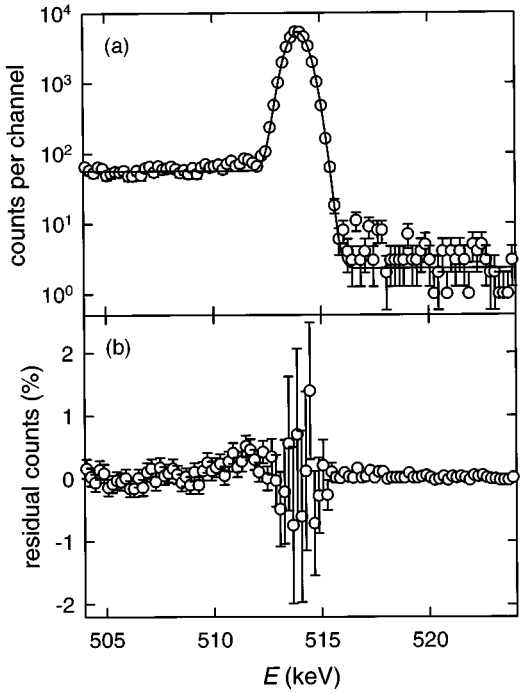

FIG. 3. (a) γ-ray spectrum of the 514.0-keV line from a ^{85}Sr source: (○) observed spectra and (—) fit to the spectrum with a combination of a Gaussian and a step function [Eq. (4)]. The linewidth is 1.16 keV. (b) Residuals of the fit.

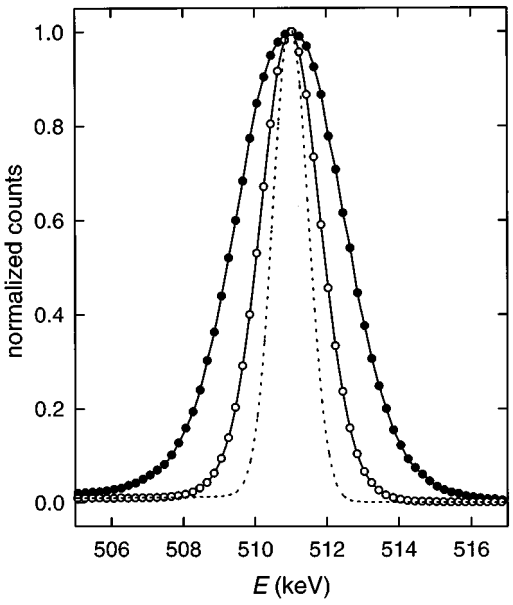

FIG. 4. Observed spectra from H_2 (○) and Ne (●) plotted on a linear scale. Solid lines are drawn to guide the eye. For the purpose of comparison, the 514.02-keV line from ^{85}Sr (dotted line) is shifted to 511 keV, which represents the detector response. The spectra are normalized to unity at the peak.

while the widths of these two lines are interpolated to find the detector energy resolution at the 511-keV line. The resolution is typically 1.16 keV.

The detector line shape was also calibrated using a ^{85}Sr source, which has a γ-ray line at 514.02 keV, conveniently close to the 511-keV line. The spectrum measured with a 3-μCi source is shown in Fig. 3(a). The fit to Eq. (4) is shown in the figure as a solid line and yields $\chi_r^2 = 1.3$. The linewidth of the Gaussian, $\Delta E_{\rm det}$, is typically 1.16 ± 0.01 keV, which agrees with the interpolated value from 344.4- and 661.6-keV lines, where 0.01 keV refers to the drift in the detector linewidth during a measurement. The residuals from the fit are shown in Fig. 3(b). These data deviate slightly from the fit on the lower-energy side of the line. This low-energy tail may be due to the trapping of electrons and/or holes in the defects of the Ge crystal [37]. Nonetheless, the residuals are generally quite small: less than 0.5% of the peak counts on the lower-energy side and even smaller ($\sim 0.1\%$) on the higher-energy side. As described in Sec. IV, these residuals are also generally much smaller than the deviations from the Gaussian shape of the observed annihilation lines. In the following, we quote the linewidth of the Gaussian fit (typically 1.16 keV) as the width of the detector response. The detector energy response and line shape vary by a small amount from day to day (typically < 0.02 keV), and a separate calibration spectrum was taken before and after each run.

IV. RESULTS

In this section, we report the results of the Doppler broadening of the γ-ray spectra from positrons annihilating on a variety of atoms and molecules in the Penning trap. The results from previous studies of momentum distributions and theoretical calculations are also tabulated and compared.

Typical spectra from our experiment are shown in Fig. 4 along with the detector response. The annihilation lines shown are the spectra from H_2 and Ne, which are the narrowest and widest lines we have observed, respectively. The observed linewidths correspond to the positrons annihilating predominantly with the valence electrons of the atoms and molecules. However, we also have evidence of annihilation on inner-shell electrons, and this will be discussed in Sec. IV I. As can be seen in Fig. 4, the detector width is substantially narrower than the observed annihilation lines. The high precision of the measurements is evident from the small scatter in the data. The total number of γ-ray counts in a spectrum is about 10^6 unless otherwise stated. For the experimentally measured spectra presented in figures, the error bars shown represent the expected statistical uncertainties in spectral amplitude due to the finite number of γ-ray counts. Spectra were recorded in 12 1-h time segments, and the linewidth was calculated from each segment. The tabulated linewidths were obtained by averaging these linewidths. The variations were typically 0.01–0.02 keV. Measurements of some substances were repeated in separate runs on different days, and those linewidths generally agree within 0.01 keV. The uncertainty in the detector response is at most 0.01 keV. We estimate the experimental precision of the linewidths to be typically 0.02 keV.

In the remainder of this section, we present annihilation line data for a variety of substances. The tables also list the annihilation rates. For some of these molecules, the annihilation rates had not been measured previously in the position trap and our measurements of them are also listed. The rates are expressed in terms of a normalized annihilation rate [7],

TABLE I. The γ-ray linewidths for noble gases obtained from Gaussian fits to the data (in keV). For comparison, experimental values from other methods as well as theoretical values are listed. The values of Z_{eff} are also quoted. (See Ref. [7] for the sources of Z_{eff} values.)

Gas	This study	Shizuma [a]	Coleman [b]	Stewart [c]	Theory (static) [d]	Theory	Z_{eff}
Helium	2.50	2.01	2.63	2.4	2.53	2.50 [e]	3.94
						2.20 [f]	
						2.45 [g]	
						2.50 [h]	
Neon	3.36	2.04	3.19	3.32	3.82	3.73 [i]	5.99
Argon	2.30	1.96	2.86	2.61	2.64	2.81 [j]	33.8
Krypton	2.09	N/A	2.65	2.63	2.36	2.50 [k]	90.1
Xenon	1.92	1.69	2.58	2.43	2.06	2.22 [k]	401

[a]Reference [32].
[b]Reference [9].
[c]Reference [30].
[d]Reference [45].
[e]Reference [24].
[f]Reference [43].
[g]Reference [38].
[h]Reference [44].
[i]Reference [39].
[j]Reference [40].
[k]Reference [41].

$$Z_{\text{eff}} \equiv \frac{\Gamma}{\pi r_0^2 c n}, \tag{7}$$

where Γ is the observed annihilation rate, r_0 is the classical radius of the electron, and n is the number density of the molecules. The experimental error of these annihilation rate measurements is limited by the difficulties in the test gas pressure measurements and estimated to be typically 20% for most substances. Detailed accounts of this type of measurement are summarized elsewhere [7]. The sources of the values are listed in Ref. [7] unless otherwise noted.

The values of the previously measured linewidths from ACAR measurements are quoted in keV as converted from the ACAR linewidths using Eq. (3).

A. Noble gases

The simple electronic structure of noble gas atoms has made them attractive candidates for studies of positron-atom interactions. Comparison between experiments [9] and theories [38–42] are available for all of these atoms. Previous theoretical calculations were based on the polarized orbital approximation, with the exception of the helium studies [24,43,44].

A qualitative understanding of the linewidths of the noble gases can be obtained by considering the simple approximation of the positron in the static potential of the atom in its Hartree-Fock ground state. While this theory gives a significant underestimate of Z_{eff}, the γ-ray linewidths are in reasonable agreement with experiment (Table I) [45]. This indicates that the momentum distribution of the electrons in the atomic ground state is the most significant factor in determining the linewidths. The experimentally measured linewidths are consistently smaller than the predictions of this simple theory.

In Table I, we compare our γ-ray spectra for noble gases with the previous measurements as well as with theoretical calculations. We note that the theoretical calculations predict the general trend of the experimental linewidths even though the calculated values differ from our measurements.

1. Helium

Helium is the simplest stable atomic gas, and it has been studied extensively. Rigorous calculations are possible for positron-helium interactions. Measurements for helium in our system are restricted by the limited capacity of our cryogenic pumps for this gas so that the data quality is not as good as those for other gases. The experimentally measured spectrum is shown in Fig. 5 together with a very recent calculation [24] using the Kohn variational method. Excellent agreement can be seen between experiment and theory, extending over three orders of magnitude in spectral amplitude. These data provide experimental evidence for deviations from the empirical Gaussian line shape described above and shown by the dashed line in Fig. 5. While such deviations are expected, previous experiments were not sufficiently precise to discern them.

2. Neon, argon, krypton, and xenon

Spectra for neon, argon, krypton, and xenon are shown in Fig. 6, and the values of the linewidths are listed in Table I. The linewidth for neon is the largest. In fact, it is the widest line we have observed for any atom or molecule. For atoms larger than neon, the linewidths decrease as the sizes of the atoms increase. Calculations using the polarized-orbital approximation are listed in Table I [39–41]. The higher momentum components in Kr as compared to Ar can be seen by the crossing of the data around 515 keV. This crossing was predicted by the static Hartree-Fock approximation, and the theory indicates that the crossing is due to a larger fraction of positrons annihilating with inner-shell electrons in Kr [45]. (Inner-shell electron annihilations will be discussed more in Sec. IV I.) The agreement between the experimental and theoretical values for these noble gases is not as good as that for helium, probably reflecting the difficulty in performing accurate calculations for all but the simplest atoms.

3. Previous measurements from other experiments

Selected values of the linewidths measured for the noble gases are listed in Table I. Stewart *et al.* [30] performed

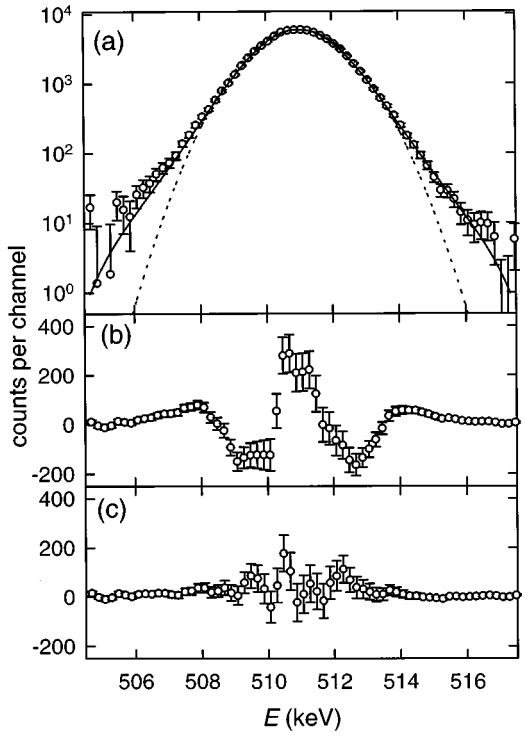

FIG. 5. (a) Annihilation γ-ray spectrum for positrons interacting with helium atoms: experimental measurements (○); theoretical prediction of Ref. [24] (—); convolved with the response of the Ge detector; Gaussian function fit to fit the experimental data (- - -). Gaussian function fit to the experimental data. (b) Residuals from the Gaussian fit. (c) Residuals from the theoretical calculation.

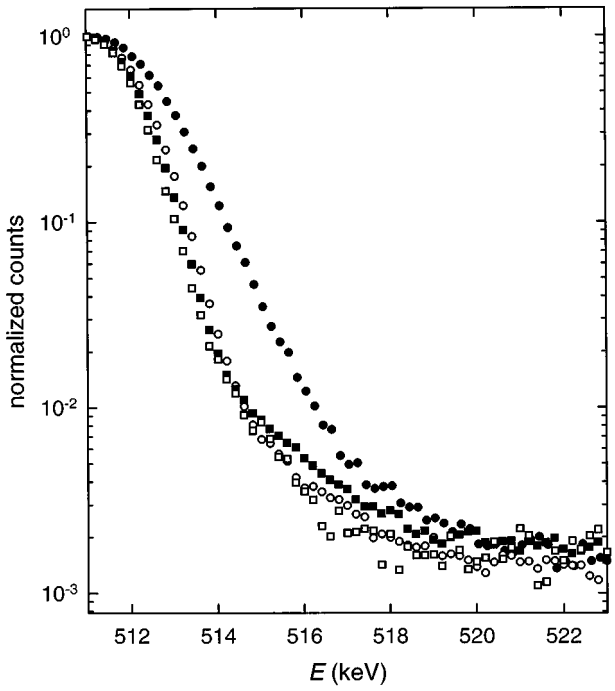

FIG. 6. Experimentally measured γ-ray spectra from noble gases: neon (●), argon (○), krypton (■), and xenon (□). The peak heights are normalized to unity. The spectra shown are for the higher-energy side of the γ-ray line since the step function in the detector response is absent in this region, and consequently the data quality is better.

ACAR measurements in condensed media, while Coleman *et al.* [9] obtained 2D ACAR measurements from gaseous targets at a pressure of 1 atm. High-energy positrons were directly injected into the gas cells in these experiments. Thus, these ACAR spectra include a contribution from the annihilation of thermalized positronium atoms. This appears as a narrow peak in the spectra, superimposed on the annihilation of free positrons on atoms, which appears as a wide component in the spectrum. The free-positron components were extracted assuming Gaussian line shapes for both contributions. The linewidths from these measurements are qualitatively similar to our measured values although the absolute values are larger. The discrepancy may come from the high sample gas pressures in the ACAR experiments, which can introduce three-body interactions. Also, the positronium contributions in the ACAR experiments were relatively large, especially for the larger noble gases, which makes the extraction of the free positron component more difficult. The only previous Doppler-broadening studies in the gas phase were reported by Shizuma *et al.* [32]. Although they did not tabulate linewidths, we have estimated numerical values from their graphical data (Table I). Their values are significantly narrower than other measurements and theoretical predictions. The reason for the discrepancy is not clear.

B. Inorganic molecules

Molecules are significantly more complicated than atoms, and consequently theoretical calculations exist for only a limited number of molecules. Experimentally measured linewidths are listed in Tables II and III for the various inorganic molecules we have studied.

1. Hydrogen

H_2 is the simplest molecule, and its significance in astrophysical positron annihilation has attracted interest from both experimentalists [15] and theorists [46,47]. The astrophysical aspects of our measurements are discussed in Sec. IV J. Our measured spectrum for hydrogen is shown in Fig. 7 along with theoretical predictions for the line shape [46,47]. The measured value of the linewidth of 1.72 ± 0.02 keV is compared with other measurements and with theoretical predictions in Table II. All experimental values and the calculated

TABLE II. The γ-ray linewidths from a Gaussian fit to the data for H_2, along with other measurements and calculations. The value of Z_{eff} is 14.6 [70].

Reference	ΔE (keV)
This study	1.71 ± 0.02
Briscoe [a]	1.66
Brown [b]	1.56 ± 0.09
Darewych [c]	1.70
Ghosh [d]	1.93

[a]ACAR measurement in liquid H_2 (6.5 mrad) [29].
[b]Doppler-broadening γ-ray spectrum measurement in gas [15].
[c]Theoretical calculation (6.65 mrad) [46].
[d]Theoretical calculation (7.54 mrad) [47].

TABLE III. The γ-ray linewidths for inorganic molecules (using Gaussian fits). (See Ref. [7] for the sources of Z_{eff} values.)

Molecule	Formula	ΔE (keV)	Z_{eff}
Nitrogen	N_2	2.32	30.5
Oxygen	O_2	2.73	36.7
Carbon monoxide	CO	2.23	38.5
Carbon dioxide	CO_2	2.63	54.7
Water	H_2O	2.59	319
Sulfur hexafluoride	SF_6	3.07	86.2
Ammonia	NH_3	2.27	1600 [a]

[a]This study.

value by Darewych are similar, while the prediction by Ghosh *et al.* is much larger than the experimental values.

2. Other gases

(a) Nitrogen. Nitrogen is the second simplest molecule. An ACAR measurement in liquid N_2 gave $\Delta E = 2.25$ keV (8.8 mrad) [30], which is in reasonable agreement with our measured value of 2.32 keV. The only theoretical calculation available gives a linewidth of 1.34 keV (5.28 mrad) [47], which is much narrower than the experimental values.

(b) Carbon monoxide and carbon dioxide. Carbon monoxide is unique in that the line shape exhibits the largest departure from a Gaussian for any molecule, as shown in Fig. 8. This is due to a small fraction of positrons annihilating with electrons having high momenta. Since this molecule is relatively simple, it may be an interesting subject for theoretical calculations. In contrast to carbon monoxide, carbon dioxide has only a weakly non-Gaussian line shape (Fig. 8).

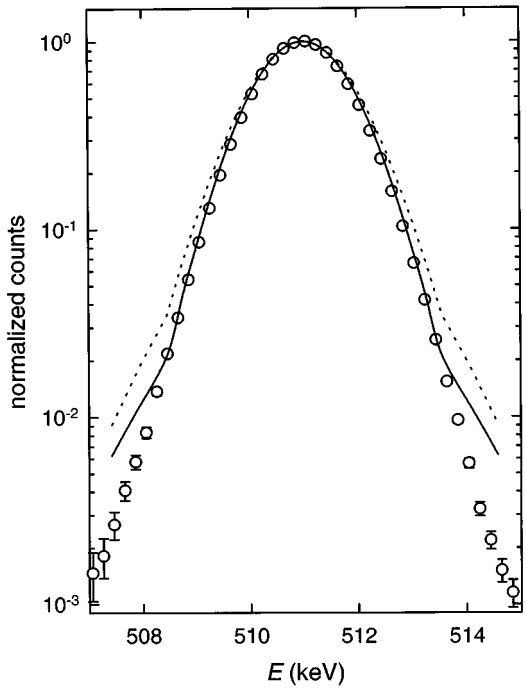

FIG. 7. γ-ray spectrum from positron annihilation on molecular hydrogen: observed spectrum (○), theoretical calculation of Ref. [46] (—), and theoretical calculation of Ref. [47] (· · ·).

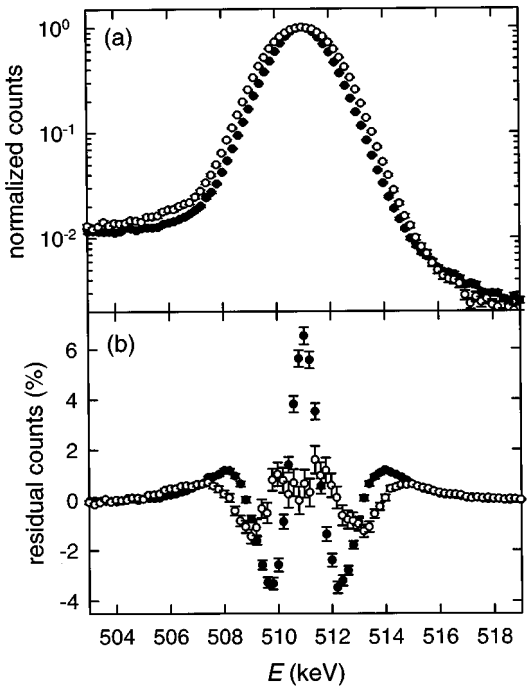

FIG. 8. (a) γ-ray spectra for positrons annihilating with CO (●) and CO_2 (○). (b) Residuals from the Gaussian fits. The data and residuals are normalized to the peak height of the spectra.

(c) Sulfur hexaflouride. Sulfur hexafluoride has very high electron affinity, and it is well known as an electron scavenger [48]. In contrast, with regard to the interaction with positrons, it has a very low annihilation rate for a molecule of this size ($Z_{\text{eff}} = 86.2$). The annihilation line is almost as wide as neon. We note that the electronic structure of the fluorine atoms in many molecules, including SF_6, is similar to the closed-shell structure of neon. Sulfur hexafluoride has a linewidth very similar to the perfluorinated alkanes. This suggests that annihilation in all of these cases occurs predominantly on the fluorine atoms, which in these molecules are electronically similar in structure to neon atoms.

(d) Ammonia. Ammonia has an anomalously large annihilation rate ($Z_{\text{eff}}/Z \sim 100$) [8]. It has a linewidth comparable to that of the alkanes. Ammonia has a considerable dipole moment, but we do not know, at present, how this would affect the linewidth. However, for more complicated molecules such as partially fluorinated hydrocarbons, we have some indication that a permanent dipole moment can have an effect on positron annihilation, as discussed in Sec. IV G.

C. Alkanes

The linewidths for the alkanes are listed in Table IV. Methane has the narrowest linewidth, 2.09 keV, and the linewidth increases to a value around 2.3 keV for large alkanes. While cyclohexane has a value of Z_{eff} about an order of magnitude smaller than hexane, the linewidth of the γ-ray spectrum is only slightly larger than that of hexane. Considering saturated hydrocarbons with five carbon atoms, there are three different isomeric configurations, and data for these molecules are shown in Table IV. While their γ-ray spectra are identical to within the experimental error, the values of annihilation rates, Z_{eff}, differ by approximately a factor of 2.

TABLE IV. The γ-ray linewidths for hydrocarbons (using Gaussian fits). (See Ref. [7] for the sources of Z_{eff} values.)

Molecule	Formula	ΔE (keV)	Z_{eff}
Alkanes			
Methane	CH_4	2.09	142
Ethane	C_2H_6	2.18	1780 [a]
Propane	C_3H_8	2.21	3500
Butane	C_4H_{10}	2.28	11 300
Pentane	C_5H_{12}	2.24	40 200 [a]
Hexane	C_6H_{14}	2.25	120 000
Nonane	C_9H_{20}	2.32	643 000
Dodecane	$C_{12}H_{26}$	2.29	1 780 000
Cyclohexane	C_6H_{12}	2.31	20 000
5-carbon alkanes			
Pentane	$CH_3(CH_2)_3CH_3$	2.24	40 200 [a]
2-Methylbutane	$CH_3C(CH_3)H_2C_2H_5$	2.23	50 500 [a]
2,2-Dimethylpropane	$C(CH_3)_4$	2.23	21 400 [a]
2-carbon molecules with different saturation level			
Ethane	C_2H_6	2.18	1780 [a]
Ethylene	C_2H_4	2.10	1200
Acetylene	C_2H_2	2.08	3160 [a]
Aromatic hydrocarbons			
Benzene	C_6H_6	2.23	15 000
Naphthalene	$C_{10}H_8$	2.29	494 000
Anthracene	$C_{14}H_{10}$	2.45	4 330 000
Toluene	$C_6H_5CH_3$	2.28	190 000

[a]This study.

In general, we have not been able to detect any systematic relationship between Z_{eff} and the linewidth for the hydrocarbons studied or for any other molecules.

In earlier work based on measurements of linewidths for four hydrocarbons, Tang *et al.* concluded that it was likely that the positrons interact primarily with C-H bond electrons in these molecules [16]. In order to test the possibility of positrons annihilating with C-C bond electrons using our improved data, we plot in Fig. 9 the linewidths ΔE as a function of the fraction of valence electrons in C-C bonds for the alkanes including cyclohexane. The fact that ΔE increases approximately linearly with the number of valence electrons in C-C bonds suggests that positrons are also annihilating with C-C bond electrons. In principle, annihilation on C-H bond electrons can be separated from annihilation on C-C bond electrons assuming that each bond has its own characteristic linewidth. Then the linear combination of these linewidths weighted by the number of bond electrons should yield the observed linewidths. From a linear regression of the data in Fig. 9, we estimate the linewidths associated with the C-H bond and C-C bond electrons to be 2.09 and 2.76 keV, respectively.

The momentum distributions for the C-C bond and C-H bond electrons have been calculated [49]. Using the graphs of the calculated momentum distributions in Ref. [49], we estimate the predicted linewidths of the C-H bond and the C-C bond to be 2.06 and 2.42 keV, respectively. The predicted linewidth for C-H bond electrons agrees reasonably well with our experimentally measured value of 2.09 keV. However, the linewidth extrapolated for the C-C bond electrons is in greater disagreement. These linewidths were calculated using the ''static'' approximation in which the effect of the positron was not included. As can be seen in the case for noble gases, wave functions without including the effect of the positron can give the qualitative estimates, but not the quantitative comparisons. Therefore, it is difficult to distinguish whether this discrepancy in the linewidth associated with the C-C bond is caused by the inadequacy in the approximation used in the calculations or by the validity of the assumption that positrons annihilate equally with any valence electron and the assumption that each bond has a characteristic linewidth.

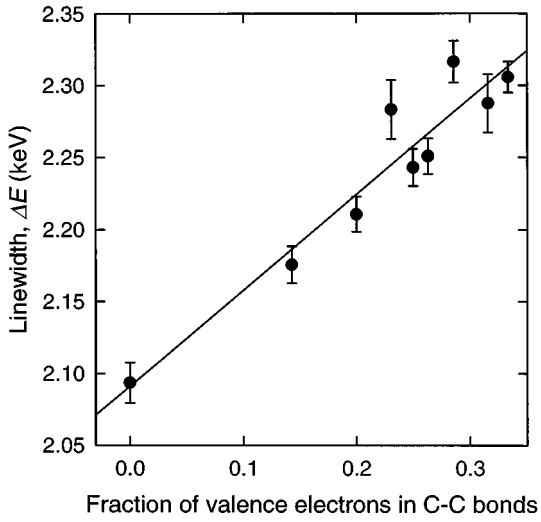

FIG. 9. The Gaussian linewidth ΔE plotted against the fraction of valence electrons in C-C bonds for alkane molecules, assuming two electrons each in the C-C and C-H bonds.

Tang *et al.* measured the linewidths of benzene, toluene, hexane, and dodecane to be 2.16, 2.15, 2.29, and 2.19 keV, respectively. Our current measurements give the linewidth of these molecules to be 2.23, 2.28, 2.25, and 2.29. The uncertainty of their measurements was 0.05 keV or larger so that the variation in the linewidths they measured were within their uncertainty. In addition, the numbers of valence electrons in C-C bonds are relatively small compared to the numbers of valence electrons in C-H bonds, which led Tang *et al.* to conclude that all hydrocarbons have the same linewidth. Given the more precise measurements presented here, it now appears that annihilation in the hydrocarbons is equally probable with any of the valence electrons including those in C-C bonds.

This is in agreement with positron annihilation momentum distributions for liquid hexane and decane measured by using ACAR techniques [49]. Calculated momentum distributions for C-H and C-C bond electrons were compared with the observed ACAR spectra, and it was concluded that positrons annihilate with both C-H and C-C bond electrons.

D. Alkane, alkene, and alkyne

Alkenes and alkynes are generally more reactive than alkanes because the π bond is weaker than the σ bond. The

TABLE V. The γ-ray linewidths for fully halogenated carbons (using Gaussian fits). (See Ref. [7] for the sources of Z_{eff} values.)

Molecule	Formula	ΔE (keV)	Z_{eff}
Carbon tetrafluoride	CF_4	3.04	54.4
Carbon tetrachloride	CCl_4	2.29	9530
Carbon tetrabromide	CBr_4	2.09	39 800

smallest members of the alkane, alkene, and alkyne families are ethane, ethylene, and acetylene, respectively. The values of the linewidths for these molecules are listed in Table IV. They show that, as the bond saturation level is reduced, the linewidths decrease. One possible explanation of this trend is that for the alkenes and alkynes, positrons can annihilate with π-bond electrons, which are less tightly bound and consequently have a smaller momentum distribution than that of the σ-bond electrons. If the assumptions are correct that each chemical bond has its own characteristic linewidth and that the linear combination of these linewidths weighted with the number of bond electrons yields the observed linewidths, the linewidth of the C-C π bond can be estimated to be 1.48 and 1.73 keV for ethylene and acetylene, respectively, using the C-H bond and C-C σ-bond values of 2.09 and 2.76 keV.

E. Aromatics

Aromatic compounds have very different electronic and geometrical structures compared to alkanes. The values of the linewidths from our measurements are listed in Table IV for the smaller aromatic molecules benzene, naphthalene, and anthracene and for some of the substituted benzenes.

The existence of polycyclic aromatic hydrocarbons (PAH) in the interstellar media has been deduced from infrared measurements [50,51]. We have found that the PAH's have very large annihilation cross sections and speculated that these molecules may contribute significantly to astrophysical positron annihilation [52]. This facet of the research is discussed in Sec. IV J. Measurements of larger PAH's, such as pyrene, were attempted, but were not successful due to the low-vapor pressure of these substances. We are planning to install a high-temperature cell in the vacuum chamber, which should make measurements of these low-vapor pressure substances possible.

F. Fully halogenated carbons

The linewidths for fully halogenated carbons are listed in Table V where we have ordered these molecules by the size of the halogen. The linewidths decrease from CF_4, to CCl_4, to CBr_4. This trend is very similar to that of the noble gas atoms; neon, argon, and krypton (Table I). In addition, the linewidths are almost identical to those of analogous noble gas atoms, particularly for the larger halogens, as one would expect if the valence electrons of the carbon atoms were completely transferred to the halogen atoms. In particular, comparing the halocarbons and noble gas atoms, the linewidths are 3.04 (3.36) for CF_4 (Ne), 2.29 (2.30) for CCl_4 (Ar), and 2.09 (2.09) for CBr_4 (Kr). These data provide evidence that, in halocarbon molecules, the positron annihilates with the valence electrons of the halogen atoms.

TABLE VI. The γ-ray linewidths for partially fluorinated hydrocarbons (using Gaussian fits).

Molecule	Formula	ΔE (keV)
Methane	CH_4	2.09
Methyl fluoride	CH_3F	2.77
Difluoromethane	CH_2F_2	2.86
Trifluoromethane	CHF_3	2.85
Carbon tetrafluoride	CF_4	3.04
Ethane	C_2H_6	2.18
Fluoroethane	C_2H_5F	2.62
1,1,1-trifluoroethane	CF_3CH_3	2.95
1,1,2-trifluoroethane	CHF_2CH_2F	2.91
1,1,1,2-tetrafluoroethane	CF_3CH_2F	3.00
1,1,2,2-tetrafluoroethane	CHF_2CHF_2	2.97
Hexafluoroethane	C_2F_6	3.04
Propane	C_3H_8	2.21
2,2-difluoropropane	$CH_3CF_2CH_3$	2.78
1,1,1-trifluoropropane	$CF_3C_2H_5$	2.86
Perfluoropropane	C_3F_8	3.05
Hexane	C_6H_{14}	2.25
1-fluorohexane	$CH_2FC_5H_{11}$	2.46
Perfluorohexane	C_6F_{14}	3.09
Benzene	C_6H_6	2.23
Fluorobenzene	C_6H_5F	2.43
1,2-difluorobenzene	$C_6H_4F_2$	2.66
1,3-difluorobenzene	$C_6H_4F_2$	2.52
1,4-difluorobenzene	$C_6H_4F_2$	2.53
1,2,4-trifluorobenzene	$C_6H_3F_3$	2.71
1,2,4,5-tetrafluorobenzene	$C_6H_2F_4$	2.77
Pentafluorobenzene	C_6HF_5	2.89
Hexafluorobenzene	C_6F_6	2.95

The differences in the linewidths for hydrocarbons and fluorocarbons are significant; hydrocarbons have large annihilation rates and relatively narrow linewidths, while perfluorocarbons have low annihilation rates and large linewidths. It was concluded by Tang *et al.* [16] that positrons annihilate predominantly with C-H bonds in hydrocarbons and with fluorine atoms in perfluorinated molecules. In order to further examine the localization of positron annihilation in a molecule, exploiting the easily distinguishable annihilation linewidths for fluorine atoms and the C-H bonds, we have studied a series of partially fluorinated hydrocarbons. These are discussed in the next section.

G. Partially fluorinated hydrocarbons

The experimentally measured γ-ray linewidths of a series of partially fluorinated hydrocarbons are summarized in Table VI, and a typical γ-ray spectrum is shown in Fig. 10(a). (We have also measured the values of Z_{eff} for these molecules and will present and discuss the implication of these measurements in a separate publication [53].) As pointed out earlier, the hydrocarbons have significantly nar-

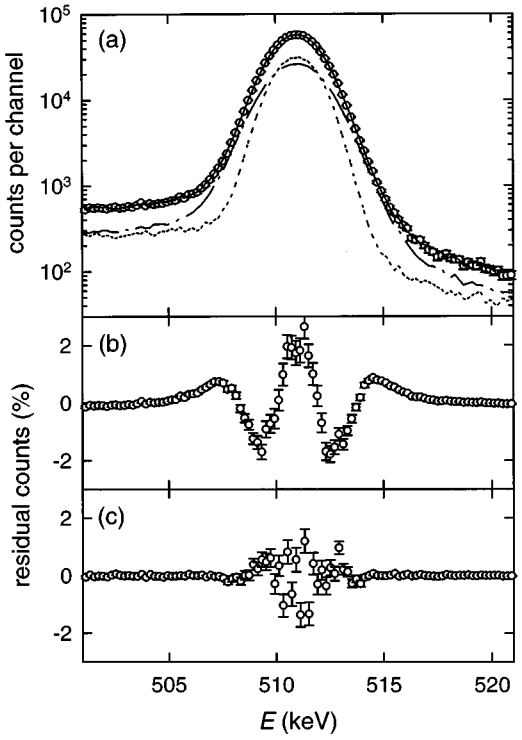

FIG. 10. γ-ray spectrum from positron annihilation on fluoroethane: (a) observed spectrum (○), and fit to the spectrum (—) using a combination of the experimentally measured ethane and hexafluoroethane spectra. The two components in the fit are also shown: the ethane spectrum (···) and the hexafluoroethane spectrum (- · -). The fraction of the area in the ethane component is 47.9%, while that in hexafluoroethane is 52.1%. (b) Residuals from a Gaussian fit ($\chi_r^2 = 28.8$) plotted as a percentage of the peak height of the spectrum. (c) Residuals from the two spectrum fit ($\chi_r^2 = 1.4$).

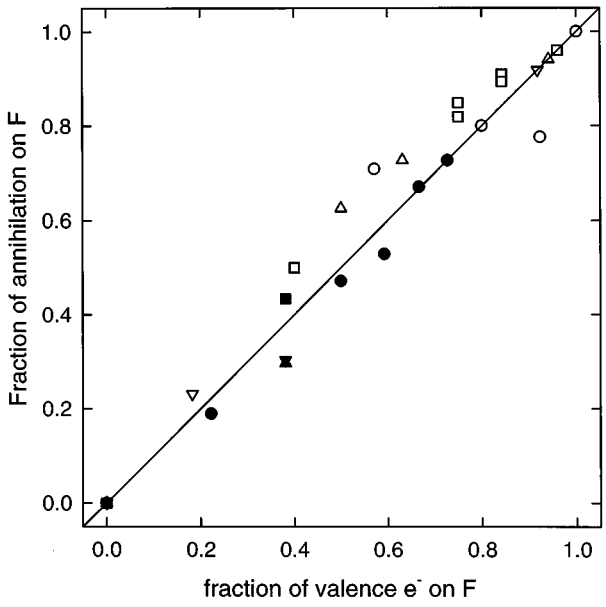

FIG. 11. Normalized fraction of positrons annihilating on fluorine atoms plotted against the fraction of the valence electrons on fluorine atoms. The fraction of annihilations on perfluorocarbons is obtained with the two-spectrum fitting procedure. This fraction is normalized with the fraction of valence electrons in fluorine atoms in the perfluorocarbons: one-carbon (i.e., methane-based) molecules (○), two-carbon (ethane-based) molecules (□), three-carbon (propane-based) molecules (△), six-carbon (hexane-based) molecules (▽). Filled symbols are for six-carbon (benzene-based) molecules with 1,2-difluorobenzene (■), 1,3-difluorobenzene (▲), 1,4-difluorobenzene (▼), and other six-carbon (benzene-based) molecules (●).

rower linewidths than the perfluorocarbons [16]. This substantial difference between the two annihilation linewidths has now made it possible for us to distinguish multiple annihilation sites in a single molecule.

For the purpose of this analysis, the annihilation line shape cannot be modeled adequately with a Gaussian, as is evident from the residuals in Fig. 10(b) and the corresponding values of χ_r^2, which are of the order of 20–40. However, at present, we do not know of an appropriate general functional form for the annihilation γ-ray line shape. Consequently, in order to separate the line shapes for the partially fluorinated hydrocarbons into two components, we fitted the spectra with a linear combination of the experimentally observed spectra for the analogous hydrocarbon and perfluorocarbon molecules. This fit has the amplitudes of the hydrocarbon and perfluorocarbon components as the only two free parameters. A typical fit and residual are shown in Figs. 10(a) and 10(c). The fit produces χ_r^2 of order of unity, indicating that the model fitting with the two experimentally measured spectra is an excellent one.

The area under the perfluorocarbon spectral component can yield the relative fraction of positrons annihilating on the fluorine atoms. This fraction is then normalized by the fraction of valence electrons on fluorine atoms in the perfluorinated molecule to take into account the annihilation on C-C bond electrons. The normalized fraction is plotted in Fig. 11 as a function of the fraction of the total number of valence electrons on the fluorine atoms. The good correlation between these two quantities suggests that the positrons annihilate with equal probability on any valence electrons. In this analysis, we have assigned eight valence electrons to each fluorine atom, assuming the formation of a closed-shell neonlike structure, and two electrons each to a C-H bond and to a C-C σ bond. For a delocalized C-C π bond in benzene, a total of six electrons is assumed in a benzene ring. We have assumed, for simplicity, that the line shape of annihilation from C-C bond electrons is the same as that from C-H bond electrons. As indicated in Sec. IV C, this is probably not strictly correct, but it is likely to be a reasonable approximation since the number of C-C bond electrons is small compared to the total number of valence electrons, and the C-C bond linewidth is not as wide as that from fluorine atoms.

The only theoretical prediction we are aware of regarding positron localization in a molecule is the study of positron attachment using approximate molecular orbital theory by Schrader and Wang [54]. A study of ethylene and its fluoro derivatives predicts that the positron is likely to be found preferentially in the vicinity of the hydrogen atoms (e.g., for C_2H_3F, 99% of the positron density is in the vicinity of the two hydrogen atoms attached to one carbon atom). Our experimental results do not seem to confirm this prediction, and the reason for the discrepancy is not clear at present.

TABLE VII. The γ-ray linewidths for other organic molecules (using Gaussian fits). (See Ref. [7] for the sources of Z_{eff} values.)

Molecule	Formula	ΔE (keV)	Z_{eff}
Methanol	CH_3OH	2.59	1510
Tetraethylsilane	$Si(C_2H_5)_4$	2.37	524 000
Nitrobenzene	$C_6H_5NO_2$	2.47	430 000
Pyridine	C_5H_5N	2.34	85 400 [a]

[a]This study.

We have measured three different isomeric configurations of difluorobenzenes. The 1,2-difluorobenzene has a higher fraction of positron annihilations on the fluorine atoms than does the 1,3- or 1,4-difluorobenzene. This may be due to the dipole moment, which is the largest for the 1,2-isomer.

H. Other organic molecules

The linewidths of four other molecules are listed in Table VII. Methanol has a Z_{eff} value an order of magnitude larger than methane. The O-H group also increases the annihilation γ-ray linewidth. Pyridine has a similar electronic structure to benzene. It has a higher Z_{eff} value and a larger linewidth.

I. Annihilation on inner-shell electrons

Our data show that positrons predominantly annihilate with the valence electrons in atoms or molecules. The potential exerted by the atomic nucleus on a positron is repulsive so that the amplitude of the positron wave function is small near the inner-shell electrons. However, a small fraction of positrons can tunnel through this repulsive potential and annihilate with inner-shell electrons. The typical linewidth from inner-shell electron annihilation is expected to be $\Delta E > 5$ keV [45], and a study of inner-shell electron annihilation requires a detailed study of this region of γ-ray spectra. Evidence of inner-shell electron annihilation can be seen in our data for Ar and Kr (Fig. 6). Using the amplitude of spectra around 516 keV, where we expect that the contribution from valence electron annihilation is small, we estimate the upper bound of the inner-shell electron annihilation contribution to be 2% and 3% for Ar and Kr, respectively. A similar analysis of carbon monoxide data indicates the upper bound on inner-shell annihilation to be 3% in this molecule, which may explain the large deviation from a Gaussian line shape discussed in Sec. IV B. This bound on inner-shell annihilation in hexane is 1%, which is smaller than those for Ar and Kr. As a consistency check, we estimate the upper bound for H_2 (which does not have inner-shell electrons) to be 0.1%, which is much smaller than those of the substances with inner-shell electrons. For Ar and Kr, Gribakin has estimated the widths and amplitudes of the annihilation on inner-shell electrons using a static Hartree-Fock approximation [45]. While this is not expected to be accurate in a quantitative sense, the widths and the amplitudes of these spectral components are consistent with this estimate.

J. Annihilation in simulated interstellar medium

The 511-keV positron annihilation line is the strongest γ-ray line of astrophysical origin [55–57]. The recent launch of the Gamma Ray Observatory has dramatically increased our knowledge of astrophysical positron annihilation [57], and high-resolution γ-ray data from a range of astrophysical sources can be expected in the next decade [58].

The narrow energy spread of the observed annihilation line is interpreted as coming from positrons that have been slowed down to a few electron volts before annihilating on either free electrons or electrons in molecules present in the interstellar medium (ISM). The physics of positron slowing and annihilation in the ISM has been the subject of both analytical models and numerical simulations [59,60]. One scenario postulates that the positrons thermalize with the ISM and then annihilate on neutral gas atoms and molecules [61]. In this case, the line shape of the γ-ray spectrum would be determined entirely by the temperature and chemical composition of the ISM.

Another scenario for the fate of astrophysical positrons involves annihilation following in-flight positronium atom formation by interaction with neutral gas atoms and molecules. In this scenario, the γ-ray line shape would be qualitatively different from that of annihilation on neutral atoms and molecules, and would depend on the dynamics of the slowing-down process. The effects of the temperature of annihilating media have also been studied theoretically [59]. Other scenarios include the effects of interstellar dust and molecular clusters [62].

Infrared observations indicate that PAH's exist in the ISM [50,51]. Because of the anomalously high annihilation rate of positrons on these molecules, we have concluded that they may contribute significantly to interstellar positron annihilation even though their molecular concentration is only about 10^{-7} that of atomic hydrogen [52]. As can be seen in Table IV, these molecules have significantly different γ-ray spectra from that of atomic hydrogen. (The linewidth for atomic hydrogen is predicted to be 1.31 keV [63].) Therefore, if cold positrons annihilate on a mixture of PAH's and hydrogen such as that expected to be present in the ISM, one could in principle distinguish the contributions to the 511-keV γ-ray annihilation line from each of these components. Using positrons in a Penning trap, we have recently been able to simulate this process. A detailed account of this work is published elsewhere [25], but we review it briefly here since it is related to the studies of the line shapes discussed in this paper.

Chrysene and triphenylene are four-ring aromatics. They are expected to be the smallest stable PAH's existing in the ISM. While we have not yet measured the annihilation rates of these specific molecules due to their low vapor pressures at room temperature, we have estimated these values by extrapolating our measurements of benzene, naphthalene, and anthracene. At room temperature we expect Z_{eff} for chrysene and triphenylene to be at least 10^7. This value is about 6 orders of magnitude larger than that of atomic hydrogen, which is calculated to be 8 around 300 K [63]. Therefore, if positrons thermalize and annihilate in the cold ISM, these PAH molecules could contribute significantly to the positron annihilation radiation despite their low concentrations.

We have measured the γ-ray spectrum from a ''simulated ISM'' consisting of a mixture of H_2 and the two-ring PAH, naphthalene, at room temperature. Even though these molecules are not likely to be the main constituents in the ISM, we expect them to produce γ-ray spectra similar to those

TABLE VIII. The fraction of annihilations on each component of a H_2-naphthalene gas mixture: Δf—calculated from a fit to data; Δf_p—calculated from measured values of pressure and Z_{eff}.

Molecule	Pressure (torr)	Z_{eff}	ΔE (keV)	Δf_p	Δf
Hydrogen	3.0×10^{-5}	14.6 [a]	1.71	21%	51%
Naphthalene	3.5×10^{-9}	494 000 [b]	2.29	79%	49%

[a]Reference [70].
[b]Reference [6].

from atomic hydrogen and the larger PAH's. The pressures of the two gases were adjusted so that their contributions to the total annihilation were approximately equal, and these values are listed in Table VIII. The observed pressure difference of 4 orders of magnitude between H_2 and naphthalene for approximately equal rates of annihilation from the two species is a striking demonstration of the extremely high annihilation rate of naphthalene.

Fitting techniques similar to those described in Sec. IV G were used to analyze this spectrum. The spectra from H_2 and from the naphthalene were measured separately, and these two spectra were used to fit the spectrum from the gas mixture. The results of the fit are listed in Table VIII. This spectral analysis produces $\chi_r^2 = 0.98$, indicating an excellent fit. By integrating the area under each component, the fractions of positrons annihilating on H_2 and on naphthalene are calculated (Table VIII). These annihilation fractions are also calculated using the measured pressures and annihilation rates. The ratio of the annihilation fraction on H_2 to that on naphthalene from the two-spectrum fitting analysis is 1 to 1, while that from the pressure measurement is 1 to 4. The difficulty in measuring the low naphthalene pressures ($\sim 10^{-9}$ Torr) using ion gauges may account for the difference.

Currently, study of the larger PAH's in a Penning trap is limited by their low vapor pressures. As mentioned above, we plan to install a high-temperature cell in the vacuum chamber. This should allow us to perform measurements on the larger PAH's, which are likely to be more abundant in the ISM. Interstellar dust and atomic clusters, which are other possible candidates for positron annihilation in the ISM [62], can also be studied in the hot cell.

In the laboratory simulation described above, we have illustrated a method for analyzing γ-ray spectra from positrons annihilating in gas mixtures. This analysis demonstrates the possibility of identifying the minority constituents of the ISM from the γ-ray spectra. In practice, such an analysis would involve building up a library of annihilation line shapes for candidate molecules and using them to fit the observed line shapes from the ISM.

V. SPECTRAL ANALYSIS BEYOND ONE-GAUSSIAN APPROXIMATION

The analyses of the measured spectra discussed thus far were done using either a single-Gaussian approximation or using a combination of the experimentally measured line shapes (e.g., in the cases of the partially fluorinated hydrocarbons and the PAH-hydrogen gas mixture). As discussed in Sec. IV, we have observed departures from Gaussian line

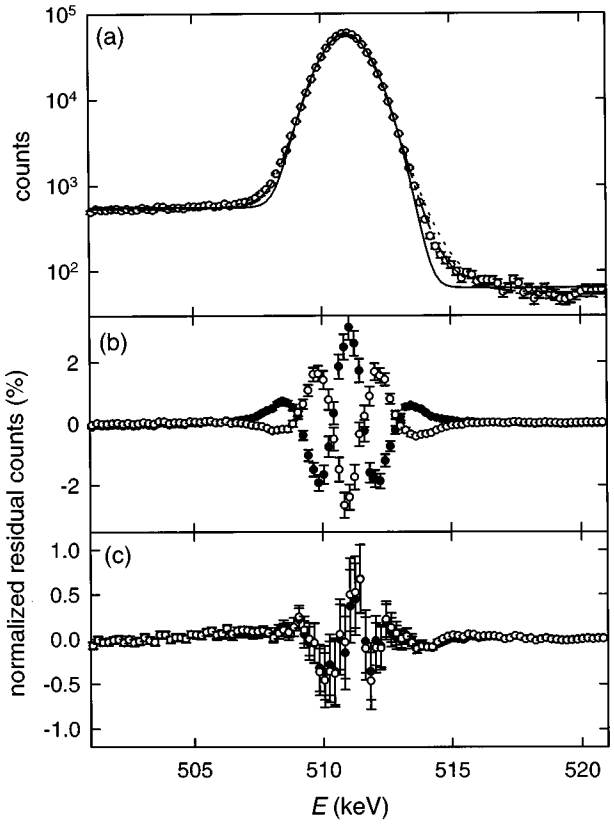

FIG. 12. (a) γ-ray spectrum of H_2: observed spectrum (○), Gaussian fit [Eq. (4)] (—), fit with noninteracting atomic hydrogen functional form [Eq. (10)] (···), and fit with Gaussian convolved non-interacting H form [Eq. (11)] (−·−). (b) Residuals from the Gaussian fit (●) and residuals from the noninteracting hydrogen fit (○). (c) Residuals from the Gaussian convolved noninteracting hydrogen fit (●) and residuals from the two-Gaussian fit [Eq. (A1)] (○).

shapes, and examples are shown in Figs. 12 and 13. We have also attempted to use other functional forms for fitting the observed spectra. Values of χ_r^2 from various fits are summarized in Table IX for hydrogen, krypton, and hexane as examples. For the hydrogen atom, in the approximation that the positron does not perturb the electron wave function, the line shape is predicted to be $1/[1+C^2(E-E_0)^2]^3$, where $C = 4\pi a_0/(hc) = 0.536\ \text{eV}^{-1}$; a_0 is the Bohr radius, and h is the Planck constant [63]. Motivated by this prediction, we convolved the function

$$g(E) = 1/[1+b(E-E_0)^2]^3 \tag{8}$$

with the detector response, which we parametrize by

$$r(E) = B_1 \exp\left[-\left(\frac{E-E_0}{a\Delta E_{\text{det}}}\right)^2\right] + B_2 \text{erfc}\left(\frac{E-E_0}{a\Delta E_{\text{det}}}\right) + B_3. \tag{9}$$

We tried to fit the resulting function,

$$G(E) = \int_0^\infty g(E')r(E-E')dE', \tag{10}$$

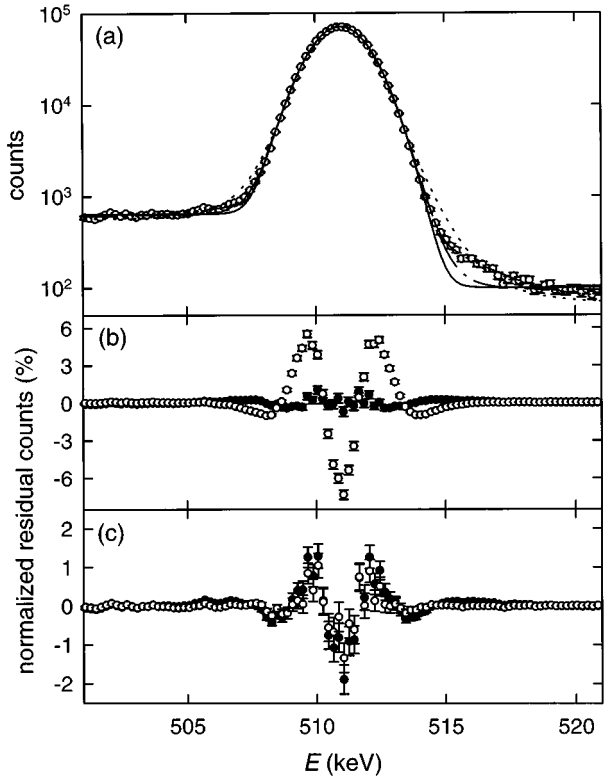

FIG. 13. (a) γ-ray spectrum of hexane (C_6H_{14}): observed spectrum (○), Gaussian fit [Eq. (4)] (—), fit with noninteracting atomic hydrogen functional form [Eq. (10)] (· · ·), fit with Gaussian convolved noninteracting H form [Eq. (11)] (− · −), and fit with two-Gaussian form [Eq. (A1)] (- - -). (b) Residuals from the Gaussian fit (●) and residuals from the noninteracting hydrogen fit (○). (c) Residuals from the Gaussian convolved noninteracting hydrogen fit (●) and residuals from the two-Gaussian fit (○).

to some of the observed spectra, using $\Delta E_{\rm det}=1.16$ keV, and E_0, B_1, B_2, B_3, and b as the fitting parameters. Examples of the fits and the residuals using Eq. (10) are shown in Figs. 12 and 13. As indicated in Table IX, these fits produced generally larger values of χ_r^2 than the Gaussian fits [Eq. (4)], especially for the hydrocarbons. Fits to the hydrogen, helium, and xenon spectra with this functional form created slightly smaller χ_r^2 values than those from the Gaussian fits, but these values are still much greater than unity.

It is interesting to note that the residuals from the Gaussian fits [Eq. (4)] are positive at the peak, while the residuals from fits with Eq. (10) are negative. A Gaussian line shape is expected from positrons annihilating with free electrons having a thermal momentum distribution. The potential exerted by the nuclei in the atoms or molecules will tend to increase the population of high momentum components of the electrons. There are two different interactions that can account for the difference between the observed spectra and the functional form Eq. (8), which is derived in the approximation that the positron does not disturb the electronic configuration of a hydrogen atom. One is the presence of the other electrons in the atom or molecule. The other is the effect of the positron on the atom or molecule. The fact that the distribution lies between the form of Eq. (8) and the Gaussian shape indicates that the distribution is more ''relaxed'' compared to Eq. (8), in other words, the distribution is more free-electron-like. The effect of other electrons seems to be strong, as can be seen by the poor fit to Eq. (10) for the case of hydrocarbons. In principle, measurement of γ-ray spectra from atomic hydrogen is possible [64], and it would indicate the magnitude of the effect of the positron on the momentum distribution.

Since the actual line shape lies somewhere between the Gaussian shape and Eq. (8), we attempted fitting another function, which is the line shape from Eq. (8), $g(E)$, convolved with a Gaussian having a variable width ΔE:

$$h(E)=\int_0^\infty g(E')\exp\left[-\left(\frac{E-E'-E_0}{a\Delta E}\right)^2\right]dE'. \qquad (11)$$

This was an attempt to take into account the degree to which electrons ''relax'' from the potential exerted by the nuclei due to the effect of the nearby positron and the many electrons in the atom or molecule. This function, $h(E)$, was then convolved with the detector response given by Eq. (9) and used for the actual fit. This function has six free parameters. As can be seen in Figs. 12(a) and 12(c), it fits spectra of some atoms and molecules reasonably well, but does not fit others, such as argon and krypton.

We have also tried to fit two Gaussians to the data. This fitting function produces values of χ_r^2 around unity, and the residuals are generally within the error bars as can be seen in Figs. 12(c) and 13(c). However, the widths of two Gaussians and the relative amplitude of the second Gaussian are highly correlated, and we know of no physical meaning for such a line shape. Nonetheless, the two-Gaussian fit is a convenient way of representing the data more accurately with an analytic form. The fitting procedure using two Gaussians is discussed in the Appendix, along with a compilation of the fitting parameters for various atoms and molecules resulting from this analysis.

VI. DISCUSSION

Previous theoretical studies of positron annihilation in gases have focused on understanding annihilation rates. This

TABLE IX. Values of χ_r^2 from fits to various models.

Molecule	One Gaussian Eq. (4)	Noninteracting H Eq. (10)	Gaussian convolved to Eq. (10) Eq. (11)	Two Gaussians Eq. (A1)
Hydrogen	14.9	9.7	1.4	2.0
Krypton	33.4	32.6	17.1	2.3
Hexane	9.9	65.0	5.8	1.4

TABLE X. γ-ray line-shape parameters from fits to two Gaussians [Eq. (A1)] for all atoms and molecules that we have studied. D is the relative amplitude of the second Gaussian.

Molecule	Formula	One-Gaussian fit χ_r^2	One-Gaussian fit ΔE	Two-Gaussian fit χ_r^2	Two-Gaussian fit ΔE_1	Two-Gaussian fit ΔE_2	D
Noble gases							
Helium	He	4.6	2.50	0.8	2.15	3.90	0.177
Neon	Ne	14.8	3.37	1.7	3.14	6.12	0.060
Argon	Ar	19.8	2.30	2.9	2.25	7.27	0.010
Krypton	Kr	33.4	2.10	2.3	2.02	6.86	0.016
Xenon	Xe	7.1	1.93	0.9	1.80	5.03	0.033
Inorganic molecules							
Hydrogen	H_2	14.9	1.71	2.0	1.50	2.65	0.153
Nitrogen	N_2	27.5	2.32	2.8	2.04	3.76	0.126
Oxygen	O_2	31.4	2.73	1.7	2.57	5.57	0.041
Carbon monoxide	CO	75.4	2.23	7.3	1.90	3.96	0.129
Carbon dioxide	CO_2	13.0	2.63	1.3	2.52	5.99	0.026
Water	H_2O	13.7	2.59	1.5	2.45	5.25	0.039
Sulfur hexafluoride	SF_6	22.8	3.07	1.9	2.91	6.56	0.034
Ammonia	NH_3	21.5	2.27	2.2	2.14	4.86	0.034
Alkanes							
Methane	CH_4	12.1	2.09	1.9	2.05	6.58	0.008
Ethane	C_2H_6	12.7	2.18	2.6	2.14	7.28	0.006
Propane	C_3H_8	9.8	2.21	1.4	2.17	6.80	0.007
Butane	C_4H_{10}	17.5	2.28	3.7	2.24	8.40	0.011
Pentane	C_5H_{12}	9.7	2.24	1.5	2.21	7.32	0.006
Hexane	C_6H_{14}	9.9	2.25	1.4	2.22	7.36	0.006
Nonane	C_9H_{20}	11.2	2.32	1.8	2.28	8.92	0.009
Dodecane	$C_{12}H_{26}$	3.0	2.29	1.0	2.27	8.53	0.005
Cyclohexane	C_6H_{12}	7.3	2.31	1.2	2.27	8.39	0.009
5-carbon alkane isomers							
2-Methylbutane	$CH_3C(CH_3)H_2C_2H_5$	13.7	2.23	1.9	2.18	7.03	0.008
2,2-Dimethylpropane	$C(CH_3)_4$	8.9	2.23	1.2	2.21	7.11	0.006
2-carbon alkene and alkyne							
Ethylene	C_2H_4	3.8	2.10	1.0	2.06	5.75	0.011
Acetylene	C_2H_2	7.0	2.08	1.3	2.00	5.11	0.021
Aromatic hydrocarbons							
Benzene	C_6H_6	15.5	2.23	2.0	2.18	6.21	0.011
Naphthalene	$C_{10}H_8$	12.3	2.29	1.9	2.25	6.62	0.011
Anthracene	$C_{14}H_{10}$	7.7	2.45	1.0	2.37	5.76	0.019
Toluene	$C_6H_5CH_3$	8.3	2.28	1.2	2.23	7.35	0.012
Halocarbons							
Carbon tetrafluoride	CF_4	31.2	3.04	2.1	2.88	6.36	0.035
Carbon tetrachloride	CCl_4	27.8	2.29	4.2	2.22	8.02	0.015
Carbon tetrabromide	CBr_4	39.9	2.09	2.8	2.00	6.52	0.018
Partially and fully fluorinated hydrocarbons							
Methyl fluoride	CH_3F	11.8	2.77	1.4	2.56	5.23	0.060
Difluoromethane	CH_2F_2	44.4	2.86	2.9	2.64	5.35	0.064
Trifluoromethane	CHF_3	33.1	2.85	2.6	2.62	5.30	0.064

TABLE X. (*Continued*).

Molecule	Formula	One-Gaussian fit χ_r^2	One-Gaussian fit ΔE	Two-Gaussian fit χ_r^2	Two-Gaussian fit ΔE_1	Two-Gaussian fit ΔE_2	Two-Gaussian fit D
Fluoroethane	C_2H_5F	28.8	2.62	1.2	2.46	5.44	0.043
1,1,1-Trifluoroethane	CF_3CH_3	33.9	2.95	2.0	2.75	5.62	0.054
1,1,2-Trifluoroethane	CHF_2CH_2F	33.9	2.91	2.0	2.73	5.73	0.049
1,1,1,2-Tetrafluoroethane	CF_3CH_2F	29.4	3.00	1.4	2.82	6.03	0.044
1,1,2,2-Tetrafluoroethane	CHF_2CHF_2	38.6	2.97	1.7	2.80	6.25	0.039
Hexafluoroethane	C_2F_6	28.2	3.04	1.9	2.88	6.28	0.036
2,2-Difluoropropane	$CH_3CF_2CH_3$	22.5	2.78	2.1	2.54	4.98	0.074
1,1,1-Trifluoropropane	$CF_3C_2H_5$	28.6	2.86	2.3	2.66	5.58	0.052
Perfluoropropane	C_3F_8	20.9	3.05	1.4	2.90	6.21	0.036
1-Fluorohexane	$CH_2FC_5H_{11}$	22.8	2.46	2.3	2.36	5.75	0.022
Perfluorohexane	C_6F_{14}	21.1	3.09	1.7	2.95	6.47	0.032
Fluorobenzene	C_6H_5F	21.5	2.43	1.4	2.31	5.47	0.027
1,2-Difluorobenzene	$C_6H_4F_2$	27.8	2.66	1.6	2.50	5.44	0.042
1,3-Difluorobenzene	$C_6H_4F_2$	30.6	2.52	1.8	2.37	5.15	0.044
1,4-Difluorobenzene	$C_6H_4F_2$	20.0	2.53	1.1	2.38	5.31	0.038
1,2,4-Trifluorobenzene	$C_6H_3F_3$	23.8	2.71	2.2	2.54	5.38	0.045
1,2,4,5-Tetrafluorobenzene	$C_6H_2F_4$	19.7	2.77	1.4	2.62	5.63	0.040
Pentafluorobenzene	C_6HF_5	26.1	2.89	1.8	2.75	6.20	0.033
Hexafluorobenzene	C_6F_6	26.5	2.95	2.6	2.81	6.45	0.030
Other organic molecules							
Methanol	CH_3OH	12.4	2.59	1.8	2.47	6.76	0.026
Tetraethylsilane	$Si(C_2H_5)_4$		2.37				
Nitrobenzene	$C_6H_5NO_2$		2.47				
Pyridine	C_5H_5N	14.1	2.34	1.5	2.24	5.19	0.026

is likely due, at least in part, to the fact that experimental data for annihilation rates are available for a variety of substances, while, previous to our positron trap experiments, there have been relatively few ACAR and γ-ray Doppler-broadening studies of atoms and molecules, except for media sufficiently dense that multiple atom and molecule effects may not be neglected. Consequently, we expect that the data presented here will be useful for comparison with the predictions of theoretical models of low-energy positron-molecule interactions. As described above, we have recently carried out such a comparison for the case of helium, resulting in excellent agreement [24].

In order to calculate either annihilation rates or γ-ray line shapes, the combined wave function for the positron and electrons must be calculated. Once the wave function is known, calculation of either the annihilation rate or the Doppler-broadened annihilation line shape is straightforward. Specific calculations that would be useful include prediction of the γ-ray spectra for annihilation on noble gases, where theory and experiment are not in good agreement except for helium, inorganic molecules such as nitrogen and carbon monoxide, which showed strong non-Gaussian features, the C-H and C-C bonds in alkanes, the σ and π bonds in aromatics such as benzene, and calculations for halocarbons.

We described an unsuccessful attempt to find a physically meaningful ''universal line shape'' beyond the single Gaussian applicable to a variety of atoms and molecules. Theoretical insights on this subject would be of value. Does such a general function exist, and if so, what is its physical interpretation?

Regarding possible improvements in experimental capabilities, we note that we now have the ability to vary the temperature of the trapped positrons in a systematic way, and we have recently carried out a study of annihilation rates in noble gases, varying the temperature of the positron gas from room temperature to about 0.6 eV [65]. Thus, in the near future, we should be able to provide data on the effect of positron temperature on γ-ray linewidths. The increased temperature of the positrons may, for example, change the fraction of annihilations at specific sites in molecules, and we will be able to search for this effect.

It is interesting to note that the temperature dependences of annihilation rates on noble gas atoms that we observed [65] agree well with calculations using the polarized-orbital approximation [38–41]. However, the absolute values of the annihilation rates [66] are underestimated in these calculations, and the predicted γ-ray linewidths (described in Sec. IV A) are larger than those observed. Thus, calculations in this approximation are capable of capturing the temperature dependences but not the absolute annihilation rates or the γ-ray spectra.

In this paper, we have presented evidence that a small fraction of positrons annihilates on inner-shell electrons. From these data, it is clear that much more can be learned by systematic studies of this effect. As noted in Sec. IV I, it is difficult to perform quantitative studies of annihilation on inner-shell electrons with our current apparatus since the Compton scattering on the low-energy tail and the pileup and sum events on the high-energy tail (which can be seen in Fig. 3) tend to mask the inner-shell annihilation signal. The technique using two high-resolution Ge detectors described by Lynn *et al.* for studies of positron annihilation in condensed media [33], which is mentioned in Sec. II B, can increase the signal-to-noise ratio in this region of the spectrum. Since inner-shell electron annihilation can now be studied experimentally, improved theoretical models for the interaction of low-energy positrons with inner-shell electrons in atoms and molecules would be useful.

Anomalously large annihilation rates for organic molecules have been known for some time [5,8]. However, the physical process responsible for this phenomenon has yet to be understood. A detailed account of the experimental work on this topic is given elsewhere [7]. We regard understanding these very large annihilation rates as an important yet unsolved problem. Here, we briefly summarize our current understanding of this problem and relate it to the measurements presented in this paper. In an attempt to understand the physical processes responsible for the high annihilation rates, we consider the following simplified model: We assume the annihilation rate can be approximated by the product of the positron-molecule collision cross section σ and the probability of annihilation during a collision. We approximate this probability by $[1-\exp(-\tau/\tau_0)]$, where τ is the duration of a collision and τ_0 is a typical annihilation time scale in matter (i.e., $\tau_0 \sim 5\times 10^{-10}$ s, which is the spin-averaged annihilation time of a positronium atom [67]). Thus,

$$Z_{\text{eff}} \propto \sigma[1-\exp(-\tau/\tau_0)]. \tag{12}$$

If σ is taken as the geometrical area of the molecule, $\sigma \sim 10^{-15}$ cm^2, and if τ is of the order of the duration of an elastic collision, $\tau \sim 10^{-15}$ s, then $Z_{\text{eff}} \sim 10$, which is much smaller than the values observed for the larger hydrocarbon molecules. Therefore, one of these quantities, σ or τ, must be much larger than the simple estimates given above. An empirical, linear scaling for nonpolar molecules without double or triple bonds was reported earlier [6] in the form

$$\log_{10}(Z_{\text{eff}}) = A(E_i - E_{\text{Ps}})^{-1} + B, \tag{13}$$

where A and B are constants, E_i is the ionization energy of the molecule, and E_{Ps} is the binding energy of a positronium atom. This suggests that the electronic structure of the molecule is important. Motivated by the empirical scaling relationship given by Eq. (13), we have suggested that the positron-molecule interaction might be thought of as a highly correlated electron-positron pair (i.e., a ''pseudopositronium atom'') bound to the molecular ion [6]. The importance of the positronium channel has been noted earlier for simple molecules [68]. However, the scaling suggests that the physics involved in the observed anomalously high annihilation rates may be dominated by this pseudopositronium atom formation. Recent large-scale calculations on organic molecules [69] lend support to this idea.

Our γ-ray spectral measurements on partially fluorinated hydrocarbons indicate that positrons annihilate with equal probability with any of the valance electrons. In addition, the data from the alkanes are also consistent with annihilation with equal probability on any valence electron. At present, we do not see how the γ-ray spectral measurements give direct information about the physical process responsible for the anomalously large annihilation rates. It is interesting to note that, as discussed in Sec. IV A, the ''static'' approximation gives reasonably good estimates for the γ-ray linewidths, but not for the annihilation rates. This may point to the importance of close-range correlation between the positron and electrons in calculating annihilation rates since the overlap in the positron and electron wave functions is involved. This correlation does not seem to be critical for the calculation of the γ-ray spectra.

Our recent annihilation rate measurements for deuterated and protonated alkanes show that the vibrational modes of molecules are not dominant factors in determining the annihilation rates [53]. Consequently, the mechanism suggested in Refs. [5,7] in which the annihilation rate was enhanced by the positron ''sticking'' to a molecule following transfer of the positron's kinetic energy to the vibrational modes of the molecule seems to be less likely. On the other hand, as noted above, the scaling of Z_{eff} with $(E_i - E_{\text{Ps}})$ given by Eq. (13) indicates that the electronic structure is very important in this process.

VII. CONCLUDING REMARKS

In this paper, we have presented measurements of the Doppler broadening of the annihilation γ-ray line, which complement other studies of positron-molecule interactions. Measurements were performed on a wide variety of substances, including noble gases, inorganic molecules, alkanes, aromatics, and substituted alkanes. The precision of the measurements is sufficiently high that one can distinguish non-Gaussian features in the line shapes. In the case of helium, the measurements are in excellent agreement with new, state-of-the-art theoretical calculations.

We have also shown that we are able to distinguish annihilation on specific sites in molecules, such as on fluorines and on C-H bonds in partially fluorinated hydrocarbons. These partially fluorinated hydrocarbon data indicate that positrons annihilate with equal probability on the valence electrons. Interpretation of our data for alkanes is also consistent with this statistical model, where the valance electrons are those in the C-H and C-C bonds in this case. We expect that the results presented in this paper for the γ-ray spectra from positron annihilation will provide useful tests of theoretical models of positron-atom and positron-molecule interactions.

Note added in proof. Recently, we have performed more careful measurements and theoretical analyses for the inner-shell annihilation on noble-gas atoms [71].

ACKNOWLEDGMENTS

We thank E. A. Jerzewski for expert technical assistance and M. Charlton, J. W. Darewych, R. J. Drachman, G. F. Gribakin, and C. Kurz for insightful discussions. This work was supported by the National Science Foundation, under Grant No. PHY-9221283, and by the Office of Naval Research.

APPENDIX: γ-RAY LINE SHAPES

As discussed in Sec. V, our measurements are precise enough to be able to study the line shapes of the spectra and not just their widths. While Gaussian line shapes are reasonable first approximations to the data, departures from a Gaussian line shape can be clearly distinguished. This can be seen from the values of χ_r^2 from fitting the Gaussian function Eq. (4) (e.g., see Table X). The values of χ_r^2, which are expected to be an order of unity for a good model, are typically around 10 or higher for the Gaussian fit. We have attempted to find a general functional form to describe the measured line shapes. However, we were unsuccessful in obtaining a functional form that is unambiguous and has physical significance. Thus, in order to present our experimental data analytically in a quantitative way, we have fitted the observed spectra with a two-Gaussian function, which is described by

$$q(E)=\exp\left[-\left(\frac{E-E_0}{a\Delta E_1}\right)^2\right]+D\exp\left[-\left(\frac{E-E_0}{a\Delta E_2}\right)^2\right] \quad \text{(A1)}$$

convolved with the detector response as given in Eq. (9). The number of free parameters is 7: E_0, ΔE_1, ΔE_2, D, B_1, B_2, and B_3. This fitting function has no physical significance of which we are aware. In addition, the Gaussian linewidths, ΔE_1 and ΔE_2, and the relative amplitude of the second Gaussian, D, are highly correlated. However, this fitting procedure yields $\chi_r^2=1-3$ (except for carbon monoxide and carbon tetrachloride), and this functional form serves the purpose of representing the experimentally measured line shapes analytically with reasonable accuracy. The fitting parameters, ΔE_1, ΔE_2, and D, are listed along with the values of χ_r^2 in Table X.

[1] A. P. Mills, Jr., Science **218**, 335 (1982).
[2] P. J. Schultz and K. G. Lynn, Rev. Mod. Phys. **60**, 701 (1988).
[3] A. Rich, Rev. Mod. Phys. **53**, 127 (1981).
[4] M. J. Puska and R. M. Nieminen, Rev. Mod. Phys. **66**, 841 (1994).
[5] C. M. Surko, M. Leventhal, and A. Passner, Phys. Rev. Lett. **62**, 901 (1989).
[6] T. J. Murphy and C. M. Surko, Phys. Rev. Lett. **67**, 2954 (1991).
[7] K. Iwata, R. G. Greaves, T. J. Murphy, M. D. Tinkle, and C. M. Surko, Phys. Rev. A **51**, 473 (1995).
[8] G. R. Heyland, M. Charlton, T. C. Griffith, and G. L. Wright, Can. J. Phys. **60**, 503 (1982).
[9] P. G. Coleman, S. Rayner, F. M. Jacobsen, M. Charlton, and R. N. West, J. Phys. B **27**, 981 (1994).
[10] A. Passner, C. M. Surko, M. Leventhal, and A. P. Mills, Jr., Phys. Rev. A **39**, 3706 (1989).
[11] G. L. Glish, R. G. Greaves, S. A. McLuckey, L. D. Hulett, C. M. Surko, J. Xu, and D. L. Donohue, Phys. Rev. A **49**, 2389 (1994).
[12] L. D. Hulett, Jr., Jun Xu, T. A. Lewis, O. H. Crawford, and S. A. McLuckey, Mat. Sci. Forum **175-178**, 687 (1995).
[13] J. Xu, L. D. Hulett, Jr., T. A. Lewis, D. L. Donohue, S. A. McLuckey, and G. L. Glish, Phys. Rev. A **47**, 1023 (1993).
[14] J. Xu, L. D. Hulett, Jr., T. A. Lewis, D. L. Donohue, S. A. McLuckey, and O. H. Crawford, Phys. Rev. A **49**, R3151 (1994).
[15] B. L. Brown and M. Leventhal, Phys. Rev. Lett. **57**, 1651 (1986).
[16] S. Tang, M. D. Tinkle, R. G. Greaves, and C. M. Surko, Phys. Rev. Lett. **68**, 3793 (1992).
[17] C. M. Surko, A. Passner, M. Leventhal, and F. J. Wysocki, Phys. Rev. Lett. **61**, 1831 (1988).
[18] R. G. Greaves and C. M. Surko, Phys. Rev. Lett. **75**, 3846 (1995).
[19] M. Charlton, J. Eades, D. Horvath, R. J. Hughes, and C. Zimmermann, Phys. Rep. **241**, 65 (1994).
[20] C. M. Surko, R. G. Greaves, and M. Charlton, Hyperfine Interact. (to be published).
[21] L. Haarsma, K. Abdullah, and G. Gabrielse, Phys. Rev. Lett. **75**, 806 (1995).
[22] A. P. Mills, Jr. and E. M. Gullikson, Appl. Phys. Lett. **49**, 1121 (1986).
[23] R. G. Greaves and C. M. Surko, Can. J. Phys. **74**, 445 (1996).
[24] P. Van Reeth, J. W. Humberston, Koji Iwata, R. G. Greaves, and C. M. Surko, J. Phys. B **29**, L465 (1996).
[25] K. Iwata, R. G. Greaves, and C. M. Surko, Can. J. Phys. **74**, 407 (1996).
[26] J. P. Peng, K. G. Lynn, P. Asoka-Kumar, and D. P. Becker, Phys. Rev. Lett. **76**, 2157 (1996).
[27] S. Berko, in *Compton Scattering*, edited by B. Williams (McGraw-Hill, London, 1977), pp. 273–322.
[28] R. N. West, J. Mayers, and P. A. Walters, J. Phys. E **14**, 478 (1981).
[29] C. V. Briscoe, S.-I. Choi, and A. T. Stewart, Phys. Rev. Lett. **20**, 493 (1968).
[30] A. T. Stewart, C. V. Briscoe, and J. J. Steinbacher, Can. J. Phys. **68**, 1362 (1990).
[31] M. Heinberg and L. A. Page, Phys. Rev. **107**, 1589 (1957).
[32] K. Shizuma, M. Nishi, T. Fujita, and Y. Yoshizawa, J. Phys. Soc. Jpn. Lett. **44**, 1757 (1978).
[33] K. G. Lynn, J. R. MacDonald, R. A. Boie, L. C. Feldman, J. D. Gabbe, M. F. Robbins, E. Bonderup, and J. Golovchenko, Phys. Rev. Lett. **38**, 241 (1977).
[34] T. J. Murphy and C. M. Surko, Phys. Rev. A **46**, 5696 (1992).
[35] R. G. Greaves, M. D. Tinkle, and C. M. Surko, Phys. Plasmas **1**, 1439 (1994).
[36] D. L. Eggleston, C. F. Driscoll, B. R. Beck, A. W. Hyatt, and J. H. Malmberg, Phys. Fluids B **4**, 3432 (1992).
[37] G. F. Knoll, *Radiation Detection and Measurement*, 2nd ed.

(John Wiley and Sons, New York, 1989).
[38] R. P. McEachran, A. G. Ryman, A. D. Stauffer, and D. L. Morgan, J. Phys. B **10**, 663 (1977); **11**, 951 (1978).
[39] R. P. McEachran, A. G. Ryman, and A. D. Stauffer, J. Phys. B **11**, 551 (1978).
[40] R. P. McEachran, A. G. Ryman, and A. D. Stauffer, J. Phys. B **12**, 1031 (1979).
[41] R. P. McEachran, A. D. Stauffer, and L. E. M. Campbell, J. Phys. B **13**, 1281 (1980).
[42] V. A. Dzuba, V. V. Flambaum, G. F. Gribakin, and W. A. King, J. Phys. B **29**, 3151 (1996).
[43] R. I. Campeanu and J. W. Humberston, J. Phys. B **10**, L153 (1977).
[44] R. J. Drachman, Phys. Rev. **179**, 237 (1969).
[45] G. F. Gribakin (private communication).
[46] J. W. Darewych, Can. J. Phys. **57**, 1027 (1979).
[47] A. S. Ghosh, T. Mukherjee, and J. W. Darewych, Hyperfine Interactions **89**, 319 (1994).
[48] J. B. Hasted and D. Mathur, in *Electron-Molecule Interactions and Their Applications*, edited by L. G. Christophorou (Academic, London, UK, 1983), Vol. 1, pp. 403–475.
[49] S. Y. Chuang and B. G. Hogg, Can. J. Phys. **45**, 3895 (1967).
[50] L. J. Allamandola, A. G. G. M. Tielens, and J. R. Barker, Astrophys. J. Lett. **290**, L25 (1985).
[51] L. J. Allamandola, A. G. G. M. Tielens, and J. R. Barker, Astrophys. J. Suppl. **71**, 733 (1989).
[52] C. M. Surko, R. G. Greaves, and M. Leventhal, Hyperfine Interactions **81**, 239 (1993).
[53] K. Iwata, G. F. Gribakin, R. G. Greaves, and C. M. Surko (unpublished).
[54] D. M. Schrader and C. M. Wang, J. Phys. Chem. **80**, 2507 (1976).
[55] R. W. Bussard, R. Ramaty, and R. J. Drachman, Astrophys. J. **228**, 928 (1979).
[56] R. Ramaty and R. E. Lingenfelter, in *High Energy Astrophysics*, edited by J. Matthews (World Scientific, New York, 1994), p. 32.
[57] W. R. Purcell, D. A. Grabelsky, M. P. Ulmer, W. N. Johnson, R. L. Kinzer, J. D. Kurfess, M. S. Strickman, and G. V. Jung, Astrophys. J. Lett. **413**, L85 (1993).
[58] A. J. Dean, Astron. Astrophys. Suppl. **97**, 361 (1993).
[59] N. Guessoum, R. Ramaty, and R. E. Lingenfelter, Astrophy. J. **378**, 170 (1991).
[60] R. J. Gould, Astrophys. J. **344**, 232 (1989).
[61] P. Wallyn, P. Durouchoux, C. Chapuis, and M. Leventhal, Astrophys. J. **422**, 610 (1994).
[62] W. H. Zurek, Astrophys. J. **289**, 603 (1985).
[63] J. W. Humberston and J. B. G. Wallace, J. Phys. B **5**, 1138 (1972).
[64] S. Zhou, W. E. Kauppila, C. K. Kwan, and T. S. Stein, Phys. Rev. Lett. **72**, 1443 (1994).
[65] C. Kurz, R. G. Greaves, and C. M. Surko, Phys. Rev. Lett. **77**, 2929 (1996).
[66] P. G. Coleman, T. C. Griffith, G. R. Heyland, and T. L. Killeen, J. Phys. B **8**, 1734 (1975).
[67] M. Charlton, Rep. Prog. Phys. **48**, 737 (1985).
[68] E. A. G. Armour, Phys. Rep. **169**, 1 (1988).
[69] E. P. de Silva, J. S. E. Germano, and M. A. P. Lima, Phys. Rev. Lett. **77**, 1028 (1996).
[70] G. Laricchia, M. Charlton, C. D. Beling, and T. C. Griffith, J. Phys. B **20**, 1865 (1987).
[71] Koji Iwata, G. F. Gribakin, R. G. Greaves, and C. M. Surko (unpublished).